Nonequilibrium transport in the pseudospin-1 Dirac-Weyl system

Cheng-Zhen Wang,[1] Hong-Ya Xu,[1] Liang Huang,[2] and Ying-Cheng Lai[1,3,*]

[1]*School of Electrical, Computer and Energy Engineering, Arizona State University, Tempe, Arizona 85287, USA*
[2]*School of Physical Science and Technology, and Key Laboratory for Magnetism and Magnetic Materials of MOE,*
Lanzhou University, Lanzhou, Gansu 730000, China
[3]*Department of Physics, Arizona State University, Tempe, Arizona 85287, USA*

Recently, solid state materials hosting pseudospin-1 quasiparticles have attracted a great deal of attention. In these materials, the energy band contains a pair of Dirac cones and a flatband through the connecting point of the cones. As the "caging" of carriers with a zero group velocity, the flatband itself has zero conductivity. However, in a nonequilibrium situation where a constant electric field is suddenly switched on, the flatband can enhance the resulting current in both the linear and nonlinear response regimes through distinct physical mechanisms. Using the $(2+1)$-dimensional pseudospin-1 Dirac-Weyl system as a concrete setting, we demonstrate that, in the weak field regime, the interband current is about twice larger than that for pseudospin-$\frac{1}{2}$ system due to the interplay between the flatband and the negative band, with the scaling behavior determined by the Kubo formula. In the strong field regime, the intraband current is $\sqrt{2}$ times larger than that in the pseudospin-$\frac{1}{2}$ system, due to the additional contribution from particles residing in the flatband. In this case, the current and field follow the scaling law associated with Landau-Zener tunneling. These results provide a better understanding of the role of the flatband in nonequilibrium transport and are experimentally testable using electronic or photonic systems.

I. INTRODUCTION

Solid state materials, due to the rich variety of their lattice structures and intrinsic symmetries [1,2], can accommodate quasiparticles that lead to quite unconventional and interesting physical phenomena. The materials and the resulting exotic quasiparticles constitute the so-called "material universe." Such materials range from graphene that hosts Dirac fermions [3] to three-dimensional (3D) topological insulators [4,5] and 3D Dirac and Weyl semimetals [6,7], in which the quasiparticles are relativistic pseudospin-$\frac{1}{2}$ fermions. Recently, Dirac-like pseudospin-1 particles have attracted much attention [8–27], which are associated with a unique type of energy band structure: a pair of Dirac cones with a flatband through the conical connecting point. Materials that can host pseudospin-1 particles include particularly engineered photonic crystals [13,16,17,19,22], optical dice or Lieb lattices with loaded ultracold atoms [8–10,12,28], and certain electronic materials [14,15,20,21]. In contrast to the Dirac cone system with massless pseudospin-$\frac{1}{2}$ particles that exhibit conventional relativistic quantum phenomena, in pseudospin-1 systems an array of quite unusual physical phenomena can arise, such as super-Klein tunneling associated with one-dimensional barrier transmission [9,11,22], diffraction-free wave propagation and novel conical diffraction [13,16,17,19], unconventional Anderson localization [27,29,30], flatband ferromagnetism [18], unconventional Landau-Zener Bloch oscillations [31], and peculiar topological phases under external gauge fields or spin-orbit coupling [12,32–34]. The aim of this paper is to present the phenomenon of enhanced nonequilibrium quantum transport of pseudospin-1 particles.

Quantum transport beyond the linear response and equilibrium regime is of great practical importance, especially in device research and development. There have been works on the nonlinear and nonequilibrium transport of relativistic pseudospin-$\frac{1}{2}$ particles in Dirac and Weyl materials. For example, when graphene is subject to a constant electric field, the dynamical evolution of the current after the field is turned on exhibits remarkable minimal conductivity behavior [35]. The scaling behavior of nonlinear electric transport in graphene due to the dynamical Landau-Zener tunneling or the Schwinger pair creation mechanism has also been investigated [36,37]. Under a strong electrical field, due to the Landau-Zener transition, a topological insulator or graphene can exhibit a quantization breakdown phenomenon in the spin Hall conductivity [38]. More recently, nonequilibrium electric transport beyond the linear response regime in 3D Weyl semimetals has been studied [39]. In these works, the quasiparticles are relativistic pseudospin-$\frac{1}{2}$ fermions arising from the Dirac or Weyl system with a conical type of dispersion in their energy momentum spectrum.

In this paper, we study the transport dynamics of pseudospin-1 quasiparticles that arise in material systems with a pair of Dirac cones and a flatband through their connecting point. Under the equilibrium condition and in the absence of disorders, the flatband acts as a perfect "caging" of carriers with zero group velocity and hence it contributes little to the conductivity [40–42]. However, as we will show in this paper, the flatband can have a significant effect on the nonequilibrium transport dynamics. Through numerical and analytic calculation of the current evolution for both weak and strong electric fields, we find the general phenomenon of current enhancement as compared with that associated with the nonequilibrium transport of pseudospin-$\frac{1}{2}$ particles. In particular, for a weak field, the interband current is twice as large as that for pseudospin-$\frac{1}{2}$ systems due to the interference between particles from the flatband and from the negative band, the scaling behavior of which agrees with that determined by the Kubo formula. For a strong field, the intraband current is

---

*ying-cheng.lai@asu.edu

115440-1

$\sqrt{2}$ times larger than that in the pseudospin-$\frac{1}{2}$ system, as a result of the additional contribution from the particles residing in the flatband. In this case, the physical origin of the scaling behavior of the current-field relation can be attributed to Landau-Zener tunneling. Our findings suggest that, in general, the conductivity of pseudospin-1 materials can be higher than that of pseudospin-$\frac{1}{2}$ materials in the nonequilibrium transport regime.

II. PSEUDOSPIN-1 HAMILTONIAN AND CURRENT

We consider a system of two-dimensional (2D) noninteracting, Dirac-like pseudospin-1 particles subject to a uniform, constant electric field applied in the x direction. The system is described by the generalized Dirac-Weyl Hamiltonian [10,24]. The electric field, switched on at $t = 0$, can be incorporated into the Hamiltonian through a time-dependent vector potential [35–39,43–45] $A(t) = [A(t),0,0]$, where $A(t) = -Et\Theta(t)$. The resulting Hamiltonian is

$$H = v_F\{S_x[p_x - qA(t)] + S_y p_y\}, \tag{1}$$

where v_F is the Fermi velocity of the pseudospin-1 particle from the Dirac cones, $q = -e$ ($e > 0$) is the electronic charge, and $S = (S_x, S_y, S_z)$ is a vector of matrices with components

$$S_x = \frac{1}{\sqrt{2}}\begin{bmatrix} 0 & 1 & 0 \\ 1 & 0 & 1 \\ 0 & 1 & 0 \end{bmatrix}, \quad S_y = \frac{1}{\sqrt{2}}\begin{bmatrix} 0 & -i & 0 \\ i & 0 & -i \\ 0 & i & 0 \end{bmatrix},$$

and

$$S_z = \begin{bmatrix} 1 & 0 & 0 \\ 0 & 0 & 0 \\ 0 & 0 & -1 \end{bmatrix}.$$

The three matrices form a complete representation of pseudospin-1 particles, which satisfy the angular momentum commutation relations $[S_l, S_m] = i\epsilon_{lmn}S_n$ with three eigenvalues, $s = \pm 1, 0$, where ϵ_{lmn} is the Levi-Civita symbol. However, the matrices do not follow the Clifford algebra underlying spin-$\frac{1}{2}$ particles. The corresponding time-dependent wave equation is

$$i\hbar\partial_t\Psi_p(t) = H\Psi_p(t). \tag{2}$$

Under the unitary transformation

$$U = \begin{bmatrix} \frac{1}{2}e^{-i\theta} & -\frac{1}{\sqrt{2}}e^{-i\theta} & \frac{1}{2}e^{-i\theta} \\ \frac{\sqrt{2}}{2} & 0 & -\frac{\sqrt{2}}{2} \\ \frac{1}{2}e^{i\theta} & \frac{1}{\sqrt{2}}e^{i\theta} & \frac{1}{2}e^{i\theta} \end{bmatrix},$$

with $\tan\theta = p_y/[p_x - qA(t)]$, we can rewrite Eq. (2) in the basis of adiabatic energy as

$$i\hbar\partial_t\Phi_p(t) = [S_z\epsilon_p(t) + S_x\sqrt{2}C_0(t)]\Phi_p(t), \tag{3}$$

where $\Phi_p(t) = U^\dagger\Psi_p(t) = [\alpha_p(t),\gamma_p(t),\beta_p(t)]^T$, $C_0(t) = \hbar v_F^2 p_y eE/\sqrt{2}\epsilon_p^2(t)$, and $\epsilon_p = v_F\sqrt{(p_x - eEt)^2 + p_y^2}$. Initially at $t = 0$, the negative band is assumed to be fully filled, $\Phi_p(t = 0) = [0,0,1]^T$. From the equation of motion, we obtain the current operator in the original basis as $J_x = -e\frac{\partial H}{\partial p_x} = -ev_F S_x$. In the transformed adiabatic energy base,

the current operator is

$$J_x = -ev_F(S_z\cos\theta - S_y\sin\theta). \tag{4}$$

We thus have the current density for a certain state as

$$\langle J_x\rangle_p(t) = -ev_F\Big\{\cos\theta\big[|\alpha_p(t)|^2 - |\beta_p(t)|^2\big]$$
$$- \sqrt{2}\sin\theta\,\mathrm{Re}\big[i\alpha_p(t)\gamma_p^*(t) + i\gamma_p(t)\beta_p^*(t)\big]\Big\}. \tag{5}$$

In Eq. (5), the first term is related to the particle number distribution associated with the positive and negative bands, which is the intraband or conduction current. The second term in Eq. (5) characterizes the interference between particles from distinct bands, which is related to the phenomenon of relativistic *zitterbewegung* and can be appropriately called the interband or polarization current.

To assess the contribution of a band (i.e., positive, flat, or negative) to the interband current, we seek to simplify the current expression. Through some algebraic substitutions, we get

$$\partial_t|\alpha_p(t)|^2 = 2\,\mathrm{Re}[\alpha_p(t)\partial_t\alpha_p^*(t)],$$
$$\partial_t|\gamma_p(t)|^2 = 2\,\mathrm{Re}[\gamma_p(t)\partial_t\gamma_p^*(t)].$$

From the Dirac equation (3), we have

$$\hbar\alpha_p(t)\partial_t\alpha_p^*(t) = i\epsilon_p\alpha_p(t)\alpha_p^*(t) + iC_0\alpha_p(t)\gamma_p^*(t),$$
$$\hbar\gamma_p(t)\partial_t\gamma_p^*(t) = iC_0\gamma_p(t)\alpha_p^*(t) + iC_0\gamma_p(t)\beta_p^*(t),$$

which gives

$$\mathrm{Re}[i\alpha_p(t)\gamma_p^*(t)] = \frac{\hbar}{2C_0}\partial_t|\alpha_p(t)|^2,$$
$$\mathrm{Re}[i\gamma_p(t)\beta_p^*(t)] = \frac{\hbar}{2C_0}[\partial_t|\alpha_p(t)|^2 + \partial_t|\gamma_p(t)|^2]. \tag{6}$$

Using the total probability conservation $|\alpha_p|^2 + |\gamma_p|^2 + |\beta_p|^2 = 1$, we finally arrive at the following current expression,

$$\langle J_x\rangle_p(t) = -ev_F\Big\{\frac{v_F(p_x - eEt)}{\epsilon_p(t)}[2|\alpha_p(t)|^2 + |\gamma_p(t)|^2 - 1]$$
$$- \frac{\epsilon_p(t)}{v_F eE}(2\partial_t|\alpha_p|^2 + \partial_t|\gamma_p|^2)\Big\}, \tag{7}$$

where the third term in the first part that is independent of the particle distribution vanishes after an integration over momentum space.

For convenience, in our numerical calculations we use dimensionless quantities, which we obtain by introducing the scale Δ, the characteristic energy of the system. The dimensionless time, electric field, momentum, energy, and coefficient are

$$\tilde{t} = \Delta t/\hbar,$$
$$\tilde{E} = ev_F\hbar E/\Delta^2,$$
$$\tilde{p} = v_F p/\Delta,$$
$$\tilde{\epsilon} = \sqrt{(\tilde{p}_x - \tilde{E}\tilde{t})^2 + \tilde{p}_y^2},$$
$$\tilde{C}_0 = \tilde{E}\tilde{p}_y/\sqrt{2}[(\tilde{p}_x - \tilde{E}\tilde{t})^2 + \tilde{p}_y^2],$$

respectively. The dimensionless current density $\tilde{J}$ can be expressed in units of $e\Delta^2/v_F\hbar^2\pi^2$. For simplicity, the spatial part of the electron wavefunction is taken into account only when we calculate total current density.

III. WEAK FIELD REGIME: ENHANCEMENT OF INTERBAND CURRENT

In the weak field regime, the intraband current is negligible as compared to the interband current due to the fewer number of conducting particles [36,37] (see Appendix B for an explanation and representative results). In particular, the interband current for a certain state can be expressed as

$$J_p^{\text{inter}} = \frac{\epsilon_p(t)}{E}\big[2\partial_t|\alpha_p|^2 + \partial_t|\gamma_p|^2\big].$$

For pseudospin-$\frac{1}{2}$ particles, the interband current has only the first term [37]. The additional term $[\epsilon_p(t)/E]\partial_t|\gamma_p|^2$ is unique for pseudospin-1 particles. To reveal the scaling behavior of the interband current and to assess the role of the positive bands and the flatbands in the current, we impose the weak field approximation $|p| = \sqrt{p_x^2 + p_y^2} \gg eEt$ everywhere except in close proximity to the Dirac point, which allows us to obtain an analytic expression for the interband current. Under the approximation, the coefficients ϵ_p and C_0 become $\epsilon_p \approx v_F p$ and $C_0 \approx \hbar p_y eE/(\sqrt{2}p^2)$, which are time independent. Substituting these approximations into Eq. (3), we obtain the three components of the time-dependent state $\Phi_p(t)$ as

$$\alpha_p(t) = \tfrac{1}{2}\big[\cos\omega t + m_0^2(\cos\omega t - 1) - 1\big], \tag{8}$$

$$\beta_p(t) = \tfrac{1}{2}\big[\cos\omega t - 2m_0\sin\omega t - m_0^2[\cos\omega t - 1] + 1\big], \tag{9}$$

$$\gamma_p(t) = \frac{1+m_0^2}{2C_0}\big[-i\hbar\omega\sin\omega t - \epsilon_p(\cos\omega t - 1)\big]. \tag{10}$$

The interband current contains two parts,

$$J_p^\alpha = 2\frac{\epsilon_p C_0^4 \omega}{E(\epsilon_p^2 + 2C_0^2)^2}(2\sin\omega t - \sin 2\omega t), \tag{11}$$

and

$$J_p^\gamma = 2\frac{\epsilon_p C_0^2 \omega}{E(\epsilon_p^2 + 2C_0^2)^2}(\epsilon_p^2\sin\omega t + C_0^2\sin 2\omega t), \tag{12}$$

which correspond to contributions from the positive band and the flatband, respectively, where $\omega = \sqrt{\epsilon_p^2 + 2C_0^2}/\hbar$. For a sufficiently weak field such that the off-diagonal term is small compared with the diagonal term in Eq. (3), we have $\epsilon_p^2 \gg 2C_0^2$, i.e.,

$$v_F^2 p^2 \gg \frac{p_y^2}{p^2}\frac{\hbar^2 e^2 E^2}{p^2}.$$

In this case, the contribution from the positive band is nearly zero and the flatband contribution is

$$J_p^\gamma \approx 2\frac{\epsilon_p^3 C_0^2 \omega}{E(\epsilon_p^2 + 2C_0^2)^2}\sin(\omega t) \approx e^2\hbar E\frac{\sin^2\theta}{p^2}\sin\left(\frac{v_F pt}{\hbar}\right). \tag{13}$$
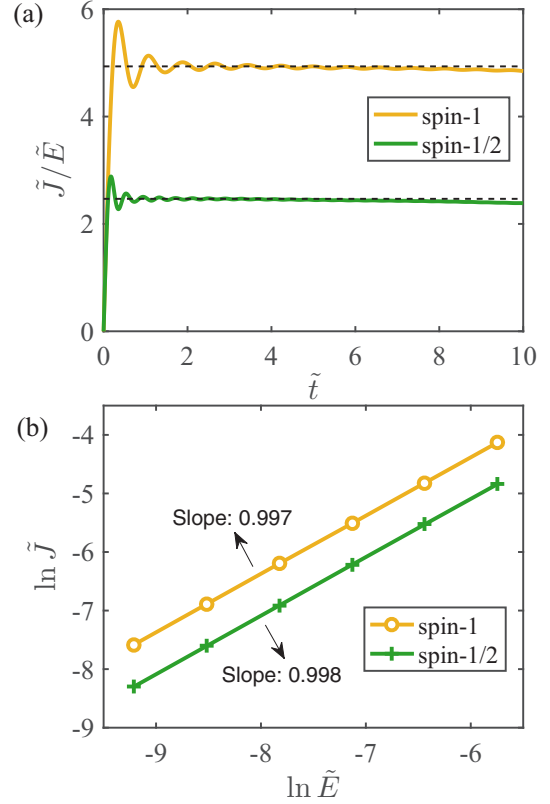

FIG. 1. Interband current in pseudospin-1 and pseudospin-$\frac{1}{2}$ systems. (a) Evolution of the total current to electric field ratio $\tilde{J}/\tilde{E}$ with time $\tilde{t}$ for pseudospin-1 and $\frac{1}{2}$ systems for a fixed electric field $\tilde{E} = 0.0004$, where the dashed lines denote the theoretical values $\pi^2/2$ and $\pi^2/4$ for the pseudospin-1 and pseudospin-$\frac{1}{2}$ systems, respectively. The yellow and green lines represent the respective numerical results. (b) The total current $\tilde{J}$ vs the electric field $\tilde{E}$ at time $\tilde{t} = 2$ for the two systems. Comparing with the pseudospin-$\frac{1}{2}$ system, the interband current in the pseudospin-1 system is greatly enhanced.

The total positive-band contribution over momentum space is negligibly small, so the flatband contributes dominantly to the total interband current density,

$$J_{\text{inter}} = \frac{1}{\pi^2\hbar^2}\iint e^2\hbar E\frac{\sin^2\theta}{p}\sin\left(\frac{v_F pt}{\hbar}\right)d\theta dp$$

$$= \frac{e^2}{2\hbar}E = \frac{e\Delta^2}{v_F\hbar^2\pi^2}\frac{\pi^2}{2}\tilde{E}. \tag{14}$$

The dimensionless current density is given by

$$\tilde{J} = \frac{\pi^2}{2}\tilde{E}. \tag{15}$$

To verify the analytical prediction Eq. (14), we calculate the interband current by numerically solving the time-dependent Dirac equation (3). For comparison, we also calculate the current for the pseudospin-$\frac{1}{2}$ system both numerically and analytically. The results are shown in Fig. 1. For the numerical results in Fig. 1(a), momentum space is defined as $\tilde{p}_x \in [-8,8]$ and $\tilde{p}_y \in [-8,8]$ and the integration grid has a spacing 0.0002. In Fig. 1(b), we use the same momentum space grid for $\tilde{E} = 0.0001, 0.0002, 0.0004$, but for $\tilde{E} = 0.0008, 0.0016, 0.0032$, the ranges of momentum space are doubled. From Fig. 1(a),
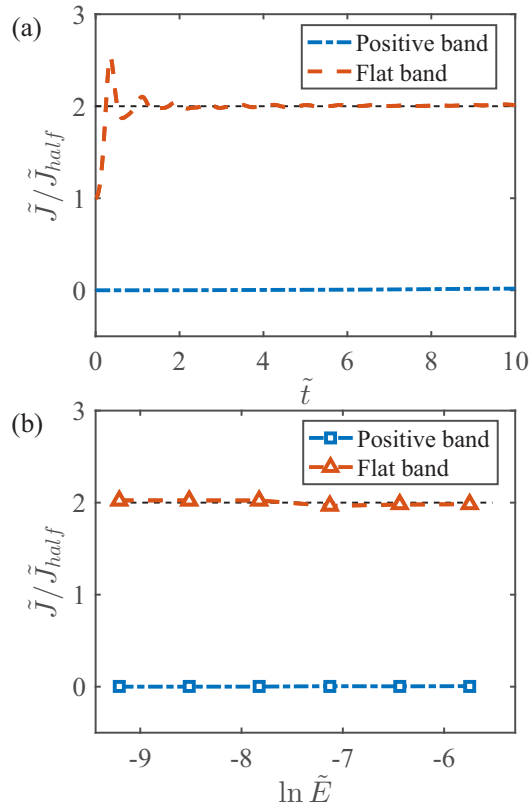
FIG. 2. Origin of interband current in the pseudospin-1 system. (a) Ratio between interband currents from the pseudospin-1 and pseudospin-$\frac{1}{2}$ systems as a function of time for electric field strength $\tilde{E} = 0.0004$, and (b) current ratio vs $\tilde{E}$ for fixed time $\tilde{t} = 2$. The black dashed lines are theoretical results, and the red and blue lines are for flatband and positive band, respectively. These results indicate that, for the pseudospin-1 system, the flatband is the sole contributor to the interband current.

we see that the interband currents for both pseudospin-1 and pseudospin-$\frac{1}{2}$ cases are independent of time. That is, after a short transient, the interband current approaches a constant. From Fig. 1(b), we see that the current is proportional to the electric field E for both pseudospin-1 and pseudospin-$\frac{1}{2}$ particles (with unity slope on a double logarithmic scale), but the proportional constant is larger in the pseudospin-1 case. While in the weak field regime, the scaling relation between the interband current and the electric field is the same for pseudospin-1 and pseudospin-$\frac{1}{2}$ particles, there is a striking difference in the current magnitude. In particular, the interband current for the pseudospin-1 system is about twice that for the pseudospin-$\frac{1}{2}$ counterpart, as revealed by both the theoretical approximation Eq. (14) and the numerical result [corresponding to the dashed and solid lines in Fig. 1(a), respectively]. The interband current in the pseudospin-1 system is thus greatly enhanced as compared to that in the pseudospin-$\frac{1}{2}$ system.

Intuitively, the phenomenon of current enhancement can be attributed to the extra flatband in the pseudospin-1 system: While the band itself does not carry any current, it can contribute to the interband current. Indeed, the theoretical results in Eqs. (11) and (12) indicate that the flatband contributes to the total interband current, while the positive band contributes
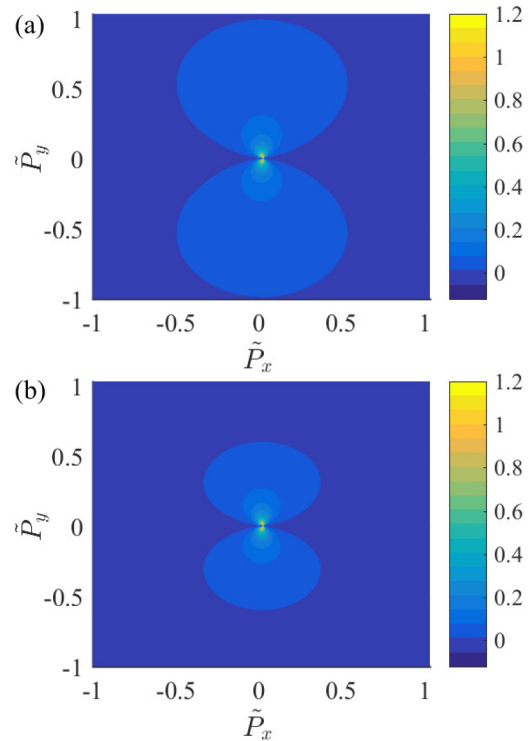

FIG. 3. Interband current distribution in momentum space: (a) pseudospin-1 and (b) pseudospin-$\frac{1}{2}$ systems. The time and electric field strength are $\tilde{t} = 2$ and $\tilde{E} = 0.0128$, respectively.

little to the current. To gain physical insights, we numerically calculate three currents: the positive-band and flatband currents from the pseudospin-1 system, and the current from the pseudospin-$\frac{1}{2}$ system. Figure 2 shows that the ratio of the flatband current to the pseudospin-$\frac{1}{2}$ current is 2, while the ratio between the positive-band and pseudospin-$\frac{1}{2}$ currents is nearly zero, indicating that in the pseudospin-1 system, almost all the interband current originates from the flatband.

To better understand the phenomenon of interband current enhancement in the pseudospin-1 system, we calculate the current distribution for both pseudospin-1 and pseudospin-$\frac{1}{2}$ systems in momentum space, as shown in Fig. 3. We see that the area in momentum space with significant current is larger for the pseudospin-1 case, although the current magnitude is almost the same near the Dirac point for both systems. This is an indication that the flatband can contribute substantially more current because the Landau-Zener transition "gap" $\tilde{p}_y$ for the pseudospin-1 system is small compared to that for the pseudospin-$\frac{1}{2}$ system. Mathematically, with respect to the single-state current expression (13) for the pseudospin-1 system, the corresponding one-state contribution to the current for the pseudospin-$\frac{1}{2}$ system is

$$J_p^{\text{half}} \approx \frac{e^2 \hbar E}{2} \frac{\sin^2 \theta}{p^2} \sin\left(\frac{2 v_F p t}{\hbar}\right). \quad (16)$$

The integration of current over the entire momentum space gives a factor of 2 enhancement for the pseudospin-1 system as compared with the pseudospin-$\frac{1}{2}$ system. This implies that quantum interference occurs mainly between particles from the negative band and flatband due to the small gap between them.

IV. STRONG FIELD REGIME: ENHANCEMENT OF INTRABAND CURRENT

In the strong field regime, the intraband current [the first term in Eq. (7)] dominates (see Appendix B). The transition probabilities for the positive band, flatband and negative band are given, respectively, by [46]

$$n_p^+ = \Theta(p_x)\Theta(eEt - p_x)\exp\left(-\frac{\pi v_F p_y^2}{\hbar e E}\right), \quad (17)$$

$$n_p^0 = \Theta(p_x)\Theta(eEt - p_x)$$
$$\times 2\left[1 - \exp\left(-\frac{\pi v_F p_y^2}{2\hbar e E}\right)\right]\left[\exp\left(-\frac{\pi v_F p_y^2}{2\hbar e E}\right)\right], \quad (18)$$

$$n_p^- = \Theta(p_x)\Theta(eEt - p_x)\left[1 - \exp\left(-\frac{\pi v_F p_y^2}{2\hbar e E}\right)\right]^2, \quad (19)$$

subject to the momentum constraint $(p_x, eEt - p_x) \gg |p_y|$. The transition probabilities are essentially the pair production or transition probabilities in the generalized three-level Landau-Zener model. Substituting Eqs. (17) and (19) into Eq. (5) [or equivalently Eq. (7)] and integrating its first term over momentum space, we obtain the positive-band contribution to the intraband current with conducting electrons (or partially filled electrons) populated from the filled bands

$$J^+ = \frac{ev_F}{\hbar^2\pi^2}\iint \frac{v_F(eEt - p_x)}{\epsilon_p(t)}|\alpha_p(t)|^2 dp_x dp_y$$
$$\approx \frac{ev_F}{\hbar^2\pi^2}\int_0^{eEt} dp_x \int_{-p_x}^{p_x} |\alpha_p(t)|^2 dp_y$$
$$\approx \frac{ev_F}{\hbar^2\pi^2}\int_0^{eEt} dp_x \int_{-\infty}^{+\infty} n_p^+(t) dp_y$$
$$= \frac{e^2}{\hbar\pi^2}\sqrt{\frac{ev_F}{\hbar}}E^{3/2}t \quad (20)$$
$$= \frac{e\Delta^2}{v_F\hbar^2\pi^2}\tilde{E}^{3/2}\tilde{t}. \quad (21)$$

The contribution to the current from the initially filled negative band with holes left by the electrons driven into the positive band and flatband, the conducting hole-based intraband current J^- is given by

$$J^- = (2\sqrt{2} - 1)\frac{e^2}{\hbar\pi^2}\sqrt{\frac{ev_F}{\hbar}}E^{3/2}t \quad (22)$$
$$= \frac{e\Delta^2}{v_F\hbar^2\pi^2}(2\sqrt{2} - 1)\tilde{E}^{3/2}\tilde{t}, \quad (23)$$

which can be written as

$$J^- = J_{\text{positive}}^- + J_{\text{flat}}^-, \quad (24)$$

where the first term accounts for the contribution by the holes left by electrons finally driven into the positive band only while the second term represents the current contribution associated with the hole concentration induced by the flatband. We have $J_{\text{positive}}^- = J^+$. The flatband-induced current results from the hole concentration in the dispersive band, which can be
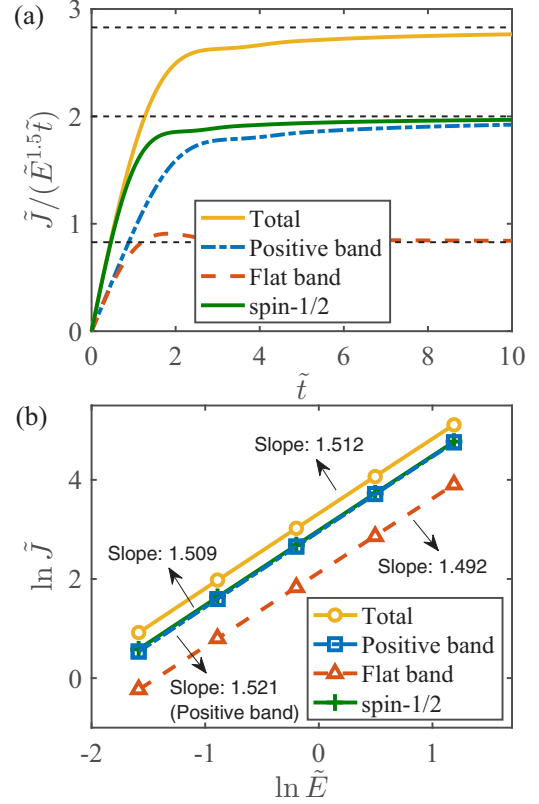

FIG. 4. Enhancement of intraband current in the strong electric field regime. Intraband current and contributions from distinct bands (a) vs time for $\tilde{E} = 0.8192$, where the black dashed lines represent the analytical values $2(\sqrt{2} - 1), 2, 2\sqrt{2}$ (from bottom) and (b) vs electric field at time $\tilde{t} = 10$ (for six values of the electric field: $\tilde{E} = 0.2048, 0.4096, 0.8192, 1.6384, 3.2768$).

written as

$$J_{\text{flat}}^- = J^- - J^+ = \frac{e\Delta^2}{v_F\hbar^2\pi^2}2(\sqrt{2} - 1)\tilde{E}^{3/2}\tilde{t}. \quad (25)$$

Taking into account both the conducting electrons and the corresponding holes, we obtain the following expression for the dispersive positive-band-based current,

$$J_{\text{positive}} = J^+ + J_{\text{positive}}^- = 2\frac{e^2}{\hbar\pi^2}\sqrt{\frac{ev_F}{\hbar}}E^{3/2}t \quad (26)$$
$$= 2\frac{e\Delta^2}{v_F\hbar^2\pi^2}\tilde{E}^{3/2}\tilde{t}. \quad (27)$$

Note that, for the pseudospin-$\frac{1}{2}$ system, this is the total current in the strong field regime [37]. The total intraband current density in the presence of the flatband in the pseudospin-1 system is

$$J^{\text{intra}} = J^+ + J^- = J_{\text{positive}} + J_{\text{flat}}^-$$
$$= 2\sqrt{2}\frac{e^2}{\hbar\pi^2}\sqrt{\frac{ev_F}{\hbar}}E^{3/2}t \quad (28)$$
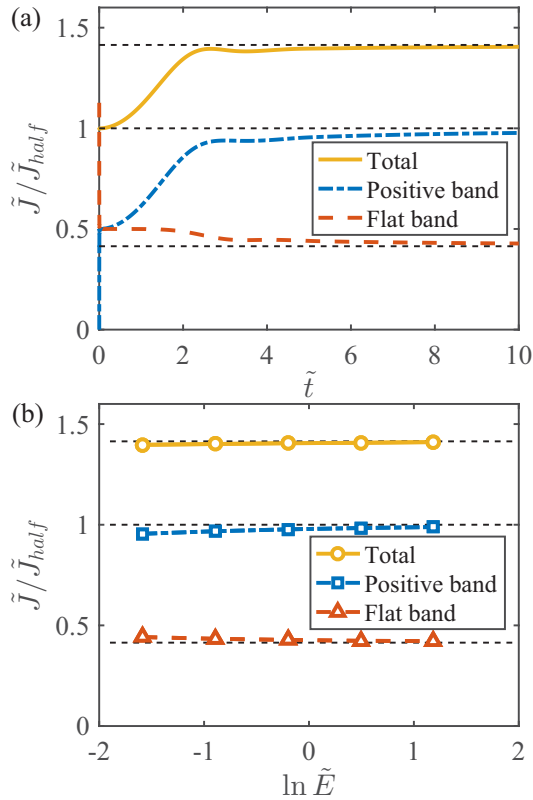$$= \frac{e\Delta^2}{v_F\hbar^2\pi^2}2\sqrt{2}\tilde{E}^{3/2}\tilde{t}. \quad (29)$$

FIG. 5. Further evidence of enhancement of intraband current in the pseudospin-1 system. (a) The ratio of the intraband currents in the pseudospin-1 and pseudospin-$\frac{1}{2}$ systems vs time $\tilde{t}$ for $\tilde{E} = 0.8192$. (b) The current ratio vs $\tilde{E}$ for $\tilde{t} = 10$.
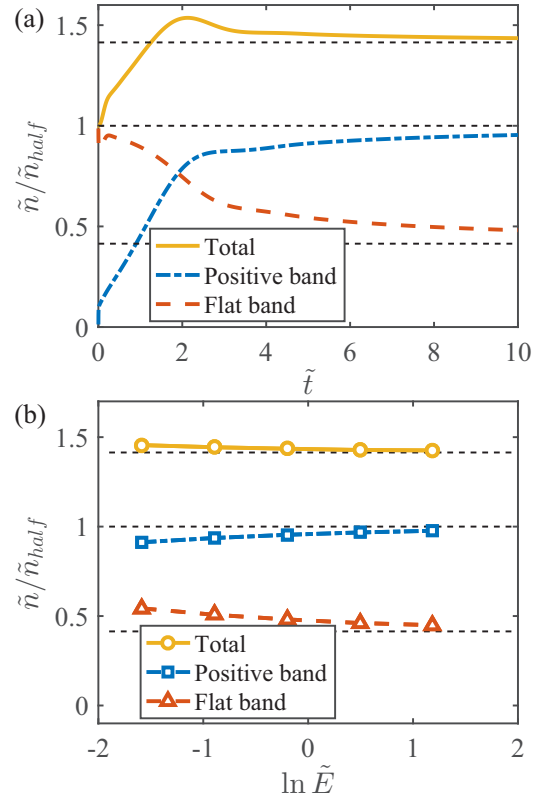

FIG. 6. Numerical evidence of pair creation mechanism for the intraband current. The ratio of particle number distribution for pseudospin-1 and pseudospin-$\frac{1}{2}$ systems (a) vs time $\tilde{t}$ for $\tilde{E} = 0.8192$ and (b) vs $\tilde{E}$ for $\tilde{t} = 10$.

Comparing with the pseudospin-$\frac{1}{2}$ case, we see that the current enhancement is due to the enhanced hole concentration as a result of the additional flatband.

The intraband current scales with the electrical field as $E^{3/2}$ and scales linearly with time, which are the same as those for the pseudospin-$\frac{1}{2}$ system [37]. However, for the pseudospin-1 system, the magnitude of the intraband current is larger: There is an enhancement factor of $\sqrt{2}$ as compared to the pseudospin-$\frac{1}{2}$ system. Since the positive-band contribution is the same as for the pseudospin-$\frac{1}{2}$ system, the enhancement is due entirely to the flatband contribution.

We now provide numerical evidence for the predicted phenomenon of intraband current enhancement in the pseudospin-1 system. Figures 4(a) and 4(b) show the intraband current $\tilde{J}$ (dimensionless) versus time $\tilde{t}$ and the electric field strength $\tilde{E}$, respectively, where the momentum space grid is $\tilde{p}_x \in [-16, 16]$ and $\tilde{p}_y \in [-16, 16]$ with spacing 0.002 in Fig. 4(a) and the momentum space range is increased according to the increase in the electric field strength in Fig. 4(b). We see that the intraband current scales with E as $E^{3/2}t$—the same as for the pseudospin-$\frac{1}{2}$ system [36,37]. There is a good agreement between the numerical results and the theoretical predictions Eqs. (21)–(29).

To provide further confirmation of the enhancement of the intraband current, we calculate the ratio between the currents from the pseudospin-1 and pseudospin-$\frac{1}{2}$ systems versus time

for certain electric fields, as shown in Fig. 5(a). The ratio versus the electric field for a given time is shown in Fig. 5(b). We see that, in the long time regime, under a strong electric field, the total intraband current for the pseudospin-1 system is about $\sqrt{2}$ times the current of the pseudospin-$\frac{1}{2}$ system. However, the positive-band currents are approximately the same for both systems. The extra current in the pseudospin-1 system, which is about 0.4 times the contribution from the positive band, originates from the flatband. These numerical results agree well with the theoretical predictions. The physical mechanism underlying the intraband current enhancement is the Schwinger mechanism or Landau-Zener tunneling [37]. Note that, in Fig. 5, the transition of an electron from the negative band to the flatband does not contribute to the intraband current, as the process leaves behind a hole in the negative band that contributes to the net current.

If the intraband current is generated by pair creation through Landau-Zener tunneling, the number of created particles should be consistent with the current behaviors. To test this, we numerically calculate the particle number distribution in different bands and plot the ratio between the numbers of particles for pseudospin-1 and pseudospin-$\frac{1}{2}$ systems versus time and the electric field, as shown in Fig. 6. For the pseudospin-1 system, the number of particles created in the positive band is approximately the same as that created in the upper band in the pseudospin-$\frac{1}{2}$ system, and the number of particles in the flatband is about half of that in the positive band.
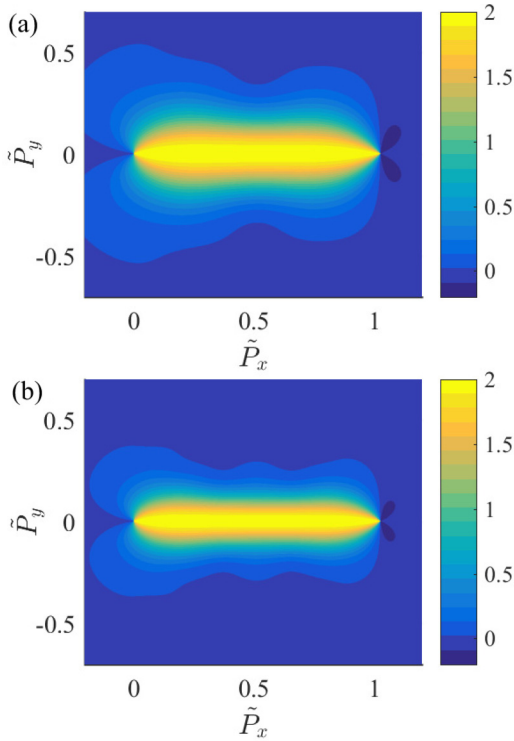
FIG. 7. Current density distribution in momentum space. (a), (b) For pseudospin-1 and pseudospin-$\frac{1}{2}$ systems, respectively, the distributions of the current density in momentum space for $\tilde{t} = 20$ and $\tilde{E} = 0.0512$. When the momentum gap value $\tilde{p}_y$ is large, the flatband can enhance the current.

Note that, for the positive band, it is necessary to count the particle number twice as both electrons and holes contribute to the transport current. However, for the flatband, only holes contribute to the current. We see that, for each band, the particle number distribution is consistent with the current distribution, providing strong evidence that the intraband current results from pair creation in the negative band. In fact, under the strong field approximation, the intraband current is the particle distributions in the positive band and flatband multiplying by the constant ev_F, as current is due to electron and hole transport.

We also calculate the current density distribution in momentum space for a fixed time and electric field strength, as shown in Fig. 7. We see that the current distribution range in the $\tilde{p}_y$ direction is wider for the pseudospin-1 system than for the pseudospin-$\frac{1}{2}$ system. However, the current distribution near $\tilde{p}_y = 0$ is approximately the same for the two systems, and the current decays in the $\tilde{p}_y$ direction. In addition, there is a current cutoff about $\tilde{p}_x = \tilde{E}\tilde{t}$ along the $\tilde{p}_x$ axis. All these features of the current density distribution can be fully explained by the theoretical formulas (17)–(19). The general result is that the flatband can enhance the current when the "gap" $\tilde{p}_y$ is large.

V. CONCLUSION AND DISCUSSION

We investigate the nonequilibrium transport of quasiparticles subject to an external electric field in the pseudospin-1 system arising from solid state materials whose energy band structure constitutes a pair of Dirac cones and a flatband

through the conical connecting point. Since the group velocity for carriers associated with the flatband is zero, one may naively think that the flatband would have no contribution to the current. However, we find that the current in the pseudospin-1 system is generally enhanced as compared with that in the counterpart (pseudospin-$\frac{1}{2}$) system. In particular, in the weak field regime, for both systems the interband current dominates, is proportional to the electric field strength, and is independent of time. However, the interference between quasiparticles associated with the flatbands and the negative bands in the pseudospin-1 system leads to an interband current whose magnitude is twice the current in the pseudospin-$\frac{1}{2}$ system. In the strong field regime, for both systems the intraband current dominates and scales with the electric field strength as $E^{3/2}$ and linearly with time. We find that the current associated with carrier transition from the negative to the positive bands is identical for both systems, but the flatband in the pseudospin-1 system contributes an additional term to the current, leading to an enhancement of the total intraband current. The general conclusion is that, from the standpoint of generating large current, the presence of the flatband in the pseudospin-1 system can be quite beneficial. Indeed, the interplay between the flatband and the Dirac cones can lead to interesting physics that has just begun to be understood and exploited.

We discuss a few pertinent issues.

Time scale of validity of effective Dirac Hamiltonian. For a real material, the effective Dirac Hamiltonian description is valid about the degeneracy (Dirac) point only, imposing an intrinsic upper bound on time in its applicability. Similar to the situation of using the two-band Dirac Hamiltonian to describe graphene [36], such a time bound can be approximately estimated as the Bloch oscillation period, i.e., the time required for the electric field to shift momentum across the Brillouin zone, $\Delta p_x = eEt \approx \hbar/a$, with a being the lattice constant. We obtain $t_B \sim \hbar/(eEa)$. Since the aim of our work is to investigate the physics near the Dirac point, the effective Hamiltonian description is sufficient. For clarity and convenience, all the calculations are done in terms of dimensionless quantities through the introduction of an auxiliary energy scale Δ whose value can be properly set to make the calculations under the restriction relevant to the real materials hosting pseudospin-1 quasiparticles. More specifically, the estimated time restriction $t < t_B$ gives rise to the following condition in terms of the dimensionless quantities,

$$\tilde{E}\tilde{t} < \frac{\hbar v_F}{\Delta a}.$$

For the given values of $\tilde{t}$ and the range of $\tilde{E}$ in all figures, the condition is fulfilled by setting $\Delta = \hbar v_F/50a$, based on which the actual physical units can be assigned to the dimensionless quantities. It is possible to test the results of this paper experimentally through tuning the characteristic energy Δ of the underlying system. While our work uses a model Hamiltonian to probe into the essential physics of pseudospin-1 systems in a relatively rigorous manner, the issue of dissipation (in momentum or energy) is beyond the intended scope of this paper.

Bloch oscillations. If the whole band structure is taken into account, Bloch oscillations will occur under an external

electric field for $t \gtrsim t_B$, i.e., the electron distribution will oscillate over a certain range of the lattice sites. In this case, the Dirac Hamiltonian description will no longer be valid. Instead, a full tight-binding Hamiltonian $H_{TB}(\boldsymbol{p})$ characterizing the multiband structure associated with a particular lattice configuration should be used. For the dice or T_3 lattice with intersite distance a and hopping integral t, the tight-binding Hamiltonian is [28]

$$H_{TB}^{(dice)}(\boldsymbol{p}) = \begin{bmatrix} 0 & h_{\boldsymbol{p}} & 0 \\ h_{\boldsymbol{p}}^* & 0 & h_{\boldsymbol{p}} \\ 0 & h_{\boldsymbol{p}}^* & 0 \end{bmatrix},$$

$$h_{\boldsymbol{p}} = -t[1 + 2\exp(3ip_y a/2)\cos(\sqrt{3}p_x a/2)].$$

A previous work [36] showed that, for the honeycomb lattice, the corresponding two-band tight-binding model can indeed give rise to Bloch oscillations for $t > t_B$. To investigate Bloch oscillations in the large time regime for pseudospin-1 systems with an extra flatband is certainly an interesting issue that warrants further efforts.

We note that, in a recent paper [31], the striking phenomenon of tunable Bloch oscillations was reported for a quasi-one-dimensional diamond lattice system with a flatband under perturbation. It would be interesting to extend this work to two-dimensional lattices. The main purpose of our work is to uncover different phenomena in physical situations where the Dirac Hamiltonian description is valid (first-order expansion of the tight-binding Hamiltonian about the Dirac points).

Effect of band anisotropy. For a particular lattice configuration associated with a real material, band anisotropy, e.g., the trigonal warping, will generally arise when entering the energy range relatively far from the Dirac points at a later time. In this case, direction-dependent transport behavior can arise. Insights into the phenomena of driving direction-resolved Bloch oscillations and Zener tunneling can be gained from existing studies of the two-band systems with the so-called "semi-Dirac" spectrum (a hybrid of the linear and quadratic dispersion) [47,48]. At present, the interplay between an additional flatband and dispersion anisotropy remains largely unknown, which is beyond the applicable scope of the idealized Dirac Hamiltonian framework.

APPENDIX A: ANALYTIC CALCULATION OF THE INTERBAND CURRENT

In the weak field regime, we can expand Eq. (3) as

$$i\hbar\partial_t\alpha_p(t) = \epsilon_p\alpha_p(t) + C_0\gamma_p(t), \tag{A1}$$

$$i\hbar\partial_t\gamma_p(t) = C_0[\alpha_p(t) + \beta_p(t)], \tag{A2}$$

$$i\hbar\partial_t\beta_p(t) = -\epsilon_p\beta_p(t) + C_0\gamma_p(t). \tag{A3}$$

Applying the time differential operator $i\hbar\partial_t$ to Eqs. (A1) and (A3), we get

$$i\hbar\partial_t[i\hbar\partial_t\alpha_p(t)] = \epsilon_p i\hbar\partial_t\alpha_p(t) + C_0 i\hbar\partial_t\gamma_p(t), \tag{A4}$$

$$i\hbar\partial_t[i\hbar\partial_t\beta_p(t)] = -\epsilon_p i\hbar\partial_t\beta_p(t) + C_0 i\hbar\partial_t\gamma_p(t), \tag{A5}$$

and, hence,

$$-\hbar^2\partial_t^2\alpha_p(t) - \hbar^2\partial_t^2\beta_p(t) = [\alpha_p(t) + \beta_p(t)][\epsilon_p^2 + 2C_0^2]. \tag{A6}$$

From Eqs. (A1) and (A3), we have

$$i\hbar\partial_t\alpha_p(t) - i\hbar\partial_t\beta_p(t) = \epsilon_p[\alpha_p(t) + \beta_p(t)]. \tag{A7}$$

Defining $x_p(t) = \alpha_p(t) + \beta_p(t)$, and $y_p(t) = \alpha_p(t) - \beta_p(t)$, we get, from Eqs. (A6) and (A7), respectively, the following relations,

$$\frac{d^2 x_p}{dt^2} + \frac{\epsilon_p^2 + 2C_0^2}{\hbar^2}x_p = 0, \tag{A8}$$

$$\frac{dy_p}{dt} = \frac{\epsilon_p}{i\hbar}x_p. \tag{A9}$$

Solving Eq. (A8), we get

$$x_p(t) = A\cos\omega t + B\sin\omega t,$$

where A and B are constant, and $\omega = \sqrt{(\epsilon_p^2 + 2C_0^2)/\hbar^2}$. Using the initial condition that the negative band is fully filled [$\Phi_p(t=0) = [0,0,1]^T$], we have $x_p(t=0) = A = 1$. From Eq. (A9), we have

$$y_p(t) = \frac{\epsilon_p}{i\hbar\omega}[\sin\omega t - B\cos\omega t] + d.$$

Using the initial condition, we get $y_p(t=0) = -m_0 B + d = -1$, where $m_0 = \epsilon_p/(i\hbar\omega)$, $d = m_0 B - 1$, which leads to

$$\alpha_p(t) = \frac{1}{2}(x+y)$$
$$= \frac{1}{2}[\cos\omega t + B\sin\omega t$$
$$+ m_0(\sin\omega t - B\cos\omega t + B) - 1],$$

$$\beta_p(t) = \frac{1}{2}(x-y)$$
$$= \frac{1}{2}[\cos\omega t + B\sin\omega t$$
$$- m_0(\sin\omega t - B\cos\omega t + B) + 1].$$

Substituting the expressions of $\alpha_p(t)$ and $\beta_p(t)$ into Eqs. (A1) and (A3), we obtain an expression for $\gamma_p(t)$. Using $\gamma_p(t=0) = 0$, we have $B = -m_0$ and, hence,

$$\alpha_p(t) = \frac{1}{2}[\cos\omega t + m_0^2(\cos\omega t - 1) - 1], \tag{A10}$$

$$\beta_p(t) = \frac{1}{2}[\cos\omega t - 2m_0\sin\omega t - m_0^2[\cos\omega t - 1] + 1], \tag{A11}$$

$$\gamma_p(t) = \frac{1+m_0^2}{2C_0}[-i\hbar\omega\sin\omega t - \epsilon_p(\cos\omega t - 1)]. \tag{A12}$$
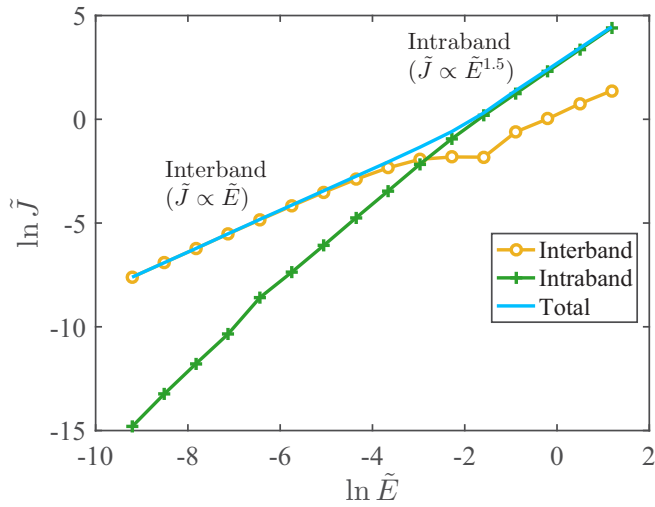
FIG. 8. Current vs electric field of pseudospin-1 system for $\tilde{t} = 5$. As the magnitude of the external electrical field is increased, the dominant contribution to the total current changes from interband to intraband, and the algebraic scaling exponent of the current-field relation changes from 1 to 1.5.

APPENDIX B: DOMINANT CURRENT SOURCE IN THE WEAK AND STRONG FIELD REGIMES

For the three-band dispersion profile investigated in this work, there are two distinct current sources, the intraband and interband currents, where the former is proportional to the number of electrons (holes) within an unfilled (occupied) band while the latter depends on the rate of change in the particle number—a characteristic of interband interference. From Eq. (7), we see that the intraband current is determined by the transition amplitudes while the interband current depends on the rate of change of the amplitudes. For a weak driving field, the transition amplitudes between the occupied and the empty bands are negligibly small, and so is the number of electron-hole generation, resulting in a weak intraband current. However, the rate of change in the transition amplitudes may not be small, and neither is the interband current. Our calculations reveal that, indeed, in the weak (strong) driving regime, the interband (intraband) current dominates. As the field is increased from the weak to the strong regime, the algebraic scaling exponent of the current-field relation changes from 1 to 1.5, as shown in Fig. 8.

[1] B. Bradlyn, J. Cano, Z. Wang, M. Vergniory, C. Felser, R. Cava, and B. A. Bernevig, Science **353**, aaf5037 (2016).

[2] C. Beenakker, Science **353**, 539 (2016).

[3] A. C. Neto, F. Guinea, N. M. Peres, K. S. Novoselov, and A. K. Geim, Rev. Mod. Phys. **81**, 109 (2009).

[4] M. Z. Hasan and C. L. Kane, Rev. Mod. Phys. **82**, 3045 (2010).

[5] X.-L. Qi and S.-C. Zhang, Rev. Mod. Phys. **83**, 1057 (2011).

[6] S.-Y. Xu, I. Belopolski, N. Alidoust, M. Neupane, G. Bian, C. Zhang, R. Sankar, G. Chang, Z. Yuan, C.-C. Lee *et al.*, Science **349**, 613 (2015).

[7] B. Lv, H. Weng, B. Fu, X. Wang, H. Miao, J. Ma, P. Richard, X. Huang, L. Zhao, G. Chen *et al.*, Phys. Rev. X **5**, 031013 (2015).

[8] D. Bercioux, D. F. Urban, H. Grabert, and W. Häusler, Phys. Rev. A **80**, 063603 (2009).

[9] R. Shen, L. B. Shao, B. Wang, and D. Y. Xing, Phys. Rev. B **81**, 041410(R) (2010).

[10] D. F. Urban, D. Bercioux, M. Wimmer, and W. Häusler, Phys. Rev. B **84**, 115136 (2011).

[11] B. Dóra, J. Kailasvuori, and R. Moessner, Phys. Rev. B **84**, 195422 (2011).

[12] N. Goldman, D. F. Urban, and D. Bercioux, Phys. Rev. A **83**, 063601 (2011).

[13] D. Guzmán-Silva, C. Mejía-Cortés, M. Bandres, M. Rechtsman, S. Weimann, S. Nolte, M. Segev, A. Szameit, and R. Vicencio, New J. Phys. **16**, 063061 (2014).

[14] W. Li, M. Guo, G. Zhang, and Y.-W. Zhang, Phys. Rev. B **89**, 205402 (2014).

[15] G. Giovannetti, M. Capone, J. van den Brink, and C. Ortix, Phys. Rev. B **91**, 121417 (2015).

[16] R. A. Vicencio, C. Cantillano, L. Morales-Inostroza, B. Real, C. Mejía-Cortés, S. Weimann, A. Szameit, and M. I. Molina, Phys. Rev. Lett. **114**, 245503 (2015).

[17] S. Mukherjee, A. Spracklen, D. Choudhury, N. Goldman, P. Öhberg, E. Andersson, and R. R. Thomson, Phys. Rev. Lett. **114**, 245504 (2015).

[18] S. Taie, H. Ozawa, T. Ichinose, T. Nishio, S. Nakajima, and Y. Takahashi, Sci. Adv. **1**, e1500854 (2015).

[19] F. Diebel, D. Leykam, S. Kroesen, C. Denz, and A. S. Desyatnikov, Phys. Rev. Lett. **116**, 183902 (2016).

[20] S. Paavilainen, M. Ropo, J. Nieminen, J. Akola, and E. Rasanen, Nano Lett. **16**, 3519 (2016).

[21] L. Zhu, S.-S. Wang, S. Guan, Y. Liu, T. Zhang, G. Chen, and S. A. Yang, Nano Lett. **16**, 6548 (2016).

[22] A. Fang, Z. Q. Zhang, S. G. Louie, and C. T. Chan, Phys. Rev. B **93**, 035422 (2016).

[23] J. D. Malcolm and E. J. Nicol, Phys. Rev. B **93**, 165433 (2016).

[24] H.-Y. Xu and Y.-C. Lai, Phys. Rev. B **94**, 165405 (2016).

[25] M. Tsuchiizu, Phys. Rev. B **94**, 195426 (2016).

[26] H. Xu and Y.-C. Lai, Phys. Rev. A **95**, 012119 (2017).

[27] A. Fang, Z. Q. Zhang, S. G. Louie, and C. T. Chan, Proc. Natl. Acad. Sci. USA **114**, 4087 (2017).

[28] A. Raoux, M. Morigi, J.-N. Fuchs, F. Piéchon, and G. Montambaux, Phys. Rev. Lett. **112**, 026402 (2014).

[29] J. T. Chalker, T. S. Pickles, and P. Shukla, Phys. Rev. B **82**, 104209 (2010).

[30] J. D. Bodyfelt, D. Leykam, C. Danieli, X. Yu, and S. Flach, Phys. Rev. Lett. **113**, 236403 (2014).

[31] R. Khomeriki and S. Flach, Phys. Rev. Lett. **116**, 245301 (2016).

[32] F. Wang and Y. Ran, Phys. Rev. B **84**, 241103 (2011).

[33] H. Aoki, M. Ando, and H. Matsumura, Phys. Rev. B **54**, R17296 (1996).

[34] C. Weeks and M. Franz, Phys. Rev. B **82**, 085310 (2010).

[35] M. Lewkowicz and B. Rosenstein, Phys. Rev. Lett. **102**, 106802 (2009).

[36] B. Rosenstein, M. Lewkowicz, H.-C. Kao, and Y. Korniyenko, Phys. Rev. B **81**, 041416 (2010).

[37] B. Dóra and R. Moessner, Phys. Rev. B **81**, 165431 (2010).

[38] B. Dóra and R. Moessner, Phys. Rev. B **83**, 073403 (2011).

[39] S. Vajna, B. Dóra, and R. Moessner, Phys. Rev. B **92**, 085122 (2015).

[40] M. Vigh, L. Oroszlány, S. Vajna, P. San-Jose, G. Dávid, J. Cserti, and B. Dóra, Phys. Rev. B **88**, 161413 (2013).

[41] W. Häusler, Phys. Rev. B **91**, 041102 (2015).

[42] T. Louvet, P. Delplace, A. A. Fedorenko, and D. Carpentier, Phys. Rev. B **92**, 155116 (2015).

[43] T. D. Cohen and D. A. McGady, Phys. Rev. D **78**, 036008 (2008).

[44] K. L. Ishikawa, Phys. Rev. B **82**, 201402 (2010).

[45] H.-C. Lee and T.-F. Jiang, J. Opt. Soc. Am. B **31**, 2263 (2014).

[46] C. Carroll and F. Hioe, J. Phys. A **19**, 1151 (1986).

[47] L.-K. Lim, J.-N. Fuchs, and G. Montambaux, Phys. Rev. Lett. **108**, 175303 (2012).

[48] L.-K. Lim, J.-N. Fuchs, and G. Montambaux, Phys. Rev. Lett. **112**, 155302 (2014).